RSC Advances

PAPER

View Article Online
View Journal | View Issue

Cite this: *RSC Adv.*, 2025, **15**, 22524

N-Acetylcysteine and pro-adrenomedullin dual-crosslinked gelatin–chitosan hydrogels with enhanced mechanical and mineralization performance†

Tonatzin Zertuche-Arias,[ab] Manuel Alatorre-Meda,[c] Ignacio A. Rivero,[d] Patricia Juárez*[a] and Ana B. Castro-Ceseña *[ae]

Bone regeneration requires coordination between bone formation, vascularization, and inflammatory regulation. However, current biomaterials often fail to provide mechanical stability and sustained bioactivity while supporting cell viability. This study presents the development and characterization of hydrogels composed of methacrylated gelatin (GelMA) and chitosan methacrylate (ChMA), crosslinked by photopolymerization (GC hydrogels). These were evaluated for their mineralization potential *in vitro* and *ex vivo* when loaded with *N*-acetylcysteine (NAC), a bioactive antioxidant (GCN); a pro-angiogenic peptide derived from adrenomedullin (PAMP, GCP); or both compounds (GCNP). FT-IR spectroscopy confirmed successful polymer methacrylation and the interaction of NAC with the polymer network. Scanning electron microscopy revealed that NAC increased the pore size from 24.49 ± 14.19 μm (GC) to 200.49 ± 80.42 μm (GCN). NAC also enhanced mechanical performance, with GCN exhibiting the highest compressive strength (151.79 ± 44.81 kPa) and GCNP the highest stiffness (Young's modulus: 55.26 ± 5.79 kPa). NAC-containing hydrogels degraded faster than GC, enabling biphasic release over 14 days. *In vitro* and *ex vivo* assays using pre-osteoblastic cells and a calvarial defect model demonstrated that GCNP hydrogels significantly enhanced cell viability and mineralization, increasing calcium deposition by 2.5-fold compared to GC ($p < 0.01$). These findings suggest that NAC not only reinforces the mechanical strength of hydrogel scaffolds designed for temporary support in non-load-bearing bone defects, but also acts as a bioactive agent upon release. Its combination with the pro-adrenomedullin peptide (PAMP) results in synergistic effects on mineralization. GCNP hydrogels are therefore promising candidates for drug delivery and bone tissue regeneration.

Received 13th May 2025
Accepted 17th June 2025

DOI: 10.1039/d5ra03349g

rsc.li/rsc-advances

1. Introduction

Bone is a highly dynamic tissue with an intrinsic ability to remodel and mineralize, which is essential for maintaining its structural integrity.[1] However, several pathological conditions such as osteoporosis, rheumatoid arthritis, vitamin D deficiency, metabolic disorders, traumatic fractures, and surgeries can disrupt these physiological processes, leading to impaired bone strength and compromised function.[2,3] Because these conditions significantly reduce patients' quality of life, a wide variety of materials have been explored to engineer three-dimensional (3D) scaffolds for bone regeneration.[4–6]

Hydrogels have emerged as promising candidates for bone tissue engineering (BTE) due to their hydrophilic polymer networks that mimic the extracellular matrix (ECM) and exhibit excellent biocompatibility, making them ideal carriers for cells and bioactive molecules.[7,8] Among these, natural polymers are of particular interest because of their structural resemblance to native ECM and biocompatibility.[9,10] Additionally, proteins and polysaccharides are biodegradable and degrade into non-toxic products. Gelatin, derived from denatured collagen—the primary structural protein in bone—is widely used in tissue engineering due to the presence of Arg-Gly-Asp (RGD)-like sequences that promote cell adhesion.[11–14] Chitosan,

[a]*Departamento de Innovación Biomédica, Centro de Investigación Científica y de Educación Superior de Ensenada, Baja California (CICESE), Carretera Ensenada-Tijuana No. 3918, Zona Playitas, C.P. 22860, Ensenada, Baja California, Mexico. E-mail: pjuarez@cicese.mx; acastro@cicese.mx*

[b]*Centro de Nanociencias y Nanotecnología, Universidad Nacional Autónoma de México, Carretera Ensenada-Tijuana Km 107, C.P. 22800, Ensenada, Baja California, Mexico*

[c]*SECIHTI-Tecnológico Nacional de México, Instituto Tecnológico de Tijuana, Centro de Graduados e Investigación en Química-Grupo de Biomateriales y Nanomedicina, Blvd. Alberto Limón Padilla S/N, C.P. 22510, Tijuana, Baja California, Mexico*

[d]*Tecnológico Nacional de México, Centro de Graduados e Investigación en Química, Tijuana 22510, BC, Mexico*

[e]*SECIHTI – Departamento de Innovación Biomédica, Centro de Investigación Científica y de Educación Superior de Ensenada, Baja California (CICESE), Carretera Ensenada-Tijuana No. 3918, Zona Playitas, C.P. 22860, Ensenada, Baja California, Mexico*

† Electronic supplementary information (ESI) available. See DOI: https://doi.org/10.1039/d5ra03349g

a polysaccharide obtained by the deacetylation of chitin, is known for its antimicrobial, hemostatic, mucoadhesive, biodegradable, and biocompatible properties. These features make it a valuable biomaterial for applications including tissue scaffolds and drug delivery systems.[15–17] However, the limited mechanical strength of natural polymers remains a significant limitation for applications in bone repair.[18–20] Methacrylation of gelatin (GelMA) and chitosan (ChMA), forms covalently crosslinked hydrogels with improved mechanical stability and broader processing flexibility across physiological temperature ranges.[21–23] Nonetheless, their functionality can be further improved by incorporating bioactive molecules that enhance their regenerative properties, particularly in bone tissue applications, where mechanical and biological cues must be carefully balanced.

To address the need for bioactive enhancement in GelMA–ChMA hydrogels, we explored the incorporation of compounds with antioxidant, anti-inflammatory, and angiogenic properties to support bone regeneration. Among them, *N*-acetylcysteine (NAC) is an antioxidant and anti-inflammatory compound with relevance in bone regeneration, where oxidative stress can impair osteogenic differentiation and bone healing.[24–26] In addition to its biological activity, NAC has been reported to play a structural role by participating in the crosslinking of methacrylate polymers and by improving cell viability, counteracting the cytotoxic effects of photoinitiators and UV exposure during polymerization.[27,28] Another promising molecule is pro-adrenomedullin N-20 peptide (PAMP), a cleavage product of adrenomedullin (AM). While AM has been widely studied in the context of bone remodeling, the role of PAMP remains largely unexplored. Notably, both peptides are implicated in processes such as inflammation, angiogenesis, and the development of mineralized tissues.[29–33] While AM has demonstrated roles in bone remodeling, the effects of PAMP remain unexplored. Interestingly, PAMP is a highly potent angiogenic factor, capable of inducing neovascularization at concentrations up to six orders of magnitude lower than vascular endothelial growth factor (VEGF) and AM.[34,35] Therefore, investigating its potential in bone regeneration becomes particularly relevant. Here, we address this knowledge gap by evaluating the effects of PAMP in this context.

This study presents the development and characterization of GelMA–ChMA hydrogels functionalized with NAC and PAMP for controlled drug delivery and enhanced bone regeneration. We systematically evaluated their chemical, morphological, mechanical, and rheological properties, along with their degradation and release profiles. Finally, the hydrogels were assessed for their ability to support pre-osteoblastic proliferation and mineralization *in vitro* and *ex vivo* using a calvaria defect model.

2. Results

To evaluate the properties of the hydrogels, we synthesized three-dimensional matrices using 4% methacrylated gelatin (GelMA) and 3% methacrylated chitosan (ChMA) at a 3 : 1 ratio, with LAP as a photoinitiator. The precursor solution that contained 20 mM NAC and 50 μg mL^{-1} PAMP was crosslinked under UV light for 60 seconds – it formed a covalently crosslinked network (Fig. 1). As a result, the obtained hydrogels exhibited a homogeneous and stable structure, whose physicochemical and biological properties were subsequently evaluated.

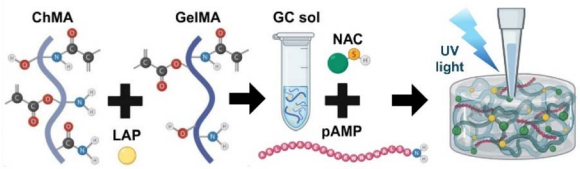

Fig. 1 Schematic representation of the hydrogel synthesis. Methacrylated chitosan (ChMA) and methacrylated gelatin (GelMA) were combined with the photoinitiator LAP to form the GC precursor solution. *N*-Acetylcysteine (NAC) and pro-adrenomedullin peptide (PAMP) were added before photopolymerization under UV light to obtain the final crosslinked hydrogel.

2.1 FTIR analysis

The FTIR analysis of freeze-dried hydrogels was conducted to assess the chemical composition of the samples and evaluate changes after methacrylation (Fig. 2A). FTIR confirmed the successful methacrylation of GelMA and ChMA, as evidenced by the appearance of characteristic bands at ~1635 cm^{-1} (C=C stretching) and ~3100–3000 cm^{-1} (weak C–H bonds). The base structures of gelatin and chitosan, including amide I (~1650 cm^{-1}) and amide II (~1550 cm^{-1}) bands were preserved.[36,37]

ChMA showed additional bands at ~1730 cm^{-1} (C=O) indicative of ester carbonyl groups from methacrylation. Post-crosslinking, the disappearance of the C=C band confirmed the consumption of methacrylate groups during polymerization.[38] In GC hydrogels, the C=C double bond band diminished, indicating the consumption of methacrylate groups during photo-crosslinking.[39] The incorporation of NAC and PAMP altered specific regions of the spectra. NAC interacted with the matrix *via* hydrogen bonding or amide bond formation, evidenced by shifts in the ~1700–1600 cm^{-1} region and the absence of SH-stretching peaks (~2550–2600 cm^{-1}) seen in free NAC.[28] PAMP modified the amide I and II regions (~1650–1550 cm^{-1}), likely through hydrogen bonding or electrostatic interactions. The combined presence of NAC and PAMP amplified these effects, suggesting synergistic interactions that influence hydrogel structure.

2.2 Microstructure of hydrogels

Porosity is a key factor in cellular penetration, attachment, proliferation, and differentiation, influencing ECM deposition, vascularization, and functional tissue formation. In BTE, smaller pores (50–100 μm) enhance cell attachment, while larger pores (200–400 μm) promote nutrient diffusion and angiogenesis.[40] Porosity analysis determined by SEM images (Fig. 2B) revealed that pore size increased significantly upon

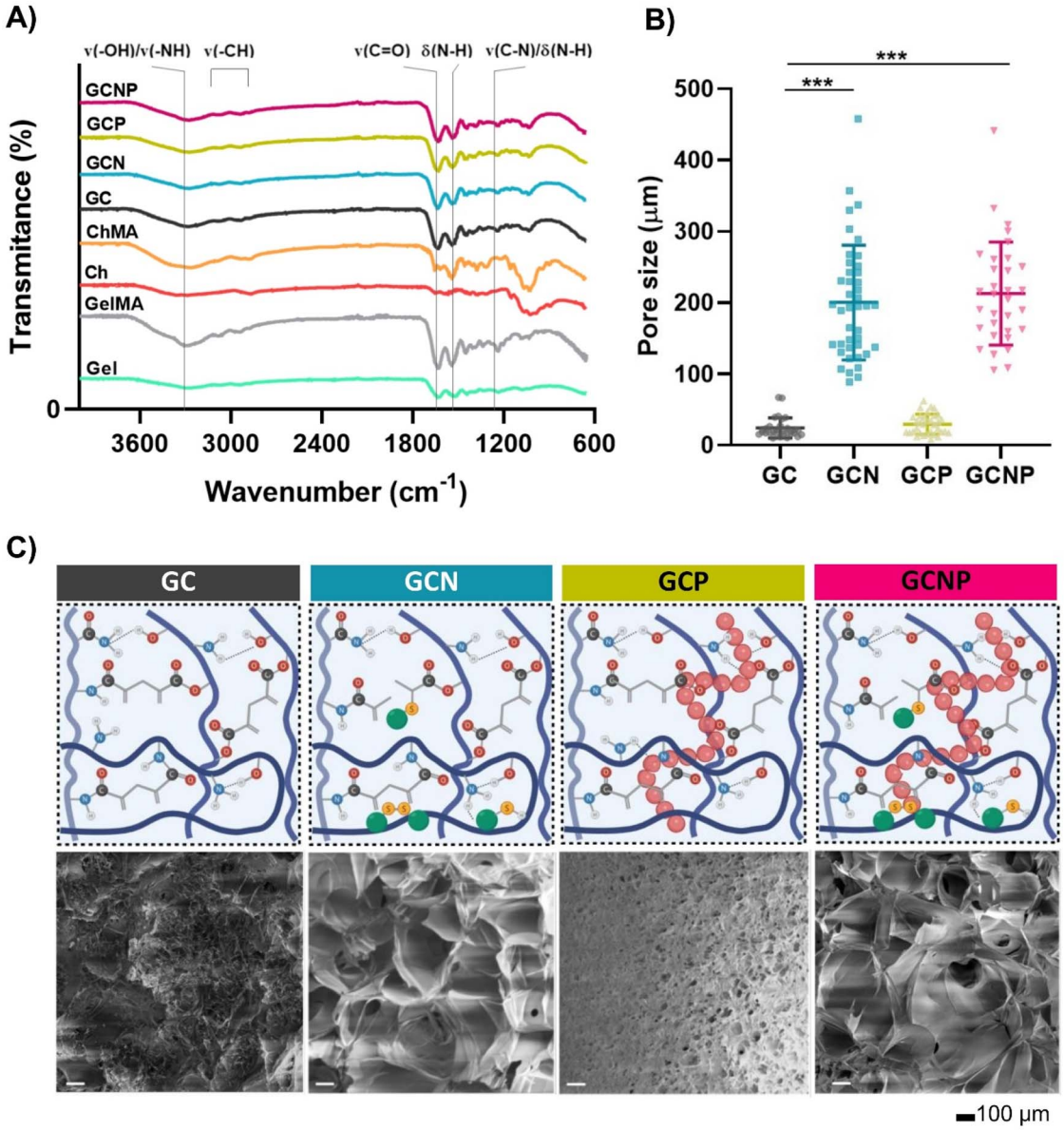

Fig. 2 Structural and chemical characterization of GC-based hydrogels. (A) FTIR spectra of unmodified (Gel, Ch), methacrylated polymers (GelMA, ChMA), and composite hydrogels (GC, GCN, GCP, GCNP). Characteristic absorption bands indicate successful methacrylation and incorporation of bioactive molecules. (B) Quantification of pore size from SEM images for each hydrogel formulation (GC: $n = 30$; GCN: $n = 42$; GCP: $n = 34$; GCNP: $n = 32$). Data are presented as mean ± standard deviation; ***$p < 0.001$. Non-significant differences between groups are not shown. (C) Schematic representations and corresponding SEM micrographs of the internal microarchitecture of GC, GCN, GCP, and GCNP hydrogels. Scale bars: 100 μm.

NAC incorporation, from 24.49 ± 14.19 μm (GC hydrogels) to 200.49 ± 80.42 μm. This trend remained consistent when PAMP was combined with NAC (212.85 ± 72.34 μm). Larger pore sizes are advantageous for nutrient diffusion, angiogenesis, and cellular infiltration, aligning with the requirements of BTE.[41] PAMP, while not significantly modifying pore size – improved the uniformity and organization of the polymer matrix (Fig. 2C).

2.3 Mechanical characterization of hydrogels

The mechanical properties of the hydrogels were evaluated through compressive stress–strain analysis, as shown in Fig. 3. The stress–strain curves (Fig. 3A) revealed distinct mechanical properties among the formulations. GC and GCP hydrogels exhibited low resistance to compressive stress, whereas GCN and GCNP displayed superior mechanical performance. Young's modulus (E) was significantly higher in GCNP (55.26 ± 5.79 kPa) compared to other formulations (Fig. 3B). Similarly, compressive strength (σF) was markedly enhanced in GCN hydrogels (151.79 ± 77.61 kPa), surpassing all other formulations (Fig. 3C). Toughness (U_T), reflecting the energy absorbed before mechanical failure, was also significantly higher in GCN hydrogels (8.9 ± 3.29 kPa), as shown in Fig. 3D. The superior

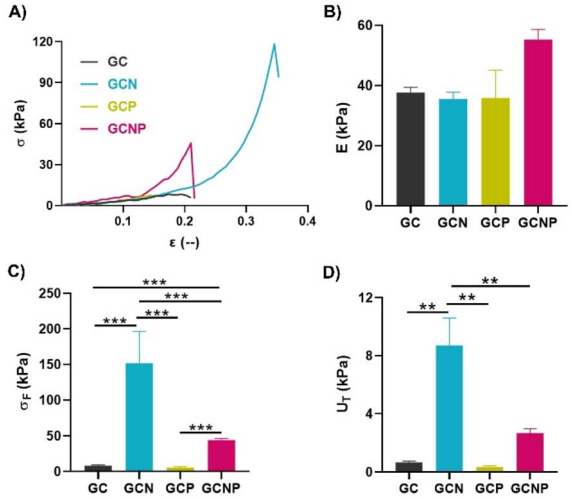

Fig. 3 Compressive mechanical properties of GC-based hydrogels. (A) Representative compressive stress–strain curves for GC, GCN, GCP, and GCNP formulations. (B) Compressive modulus (E), (C) maximum compressive strength (σF), and (D) total energy absorbed (U_T). Data are presented as mean ± standard deviation ($n = 3$). Statistical significance is indicated as follows: $p < 0.05$ (*), $p < 0.01$ (**), and $p < 0.001$ (***). Differences without asterisks are not statistically significant.

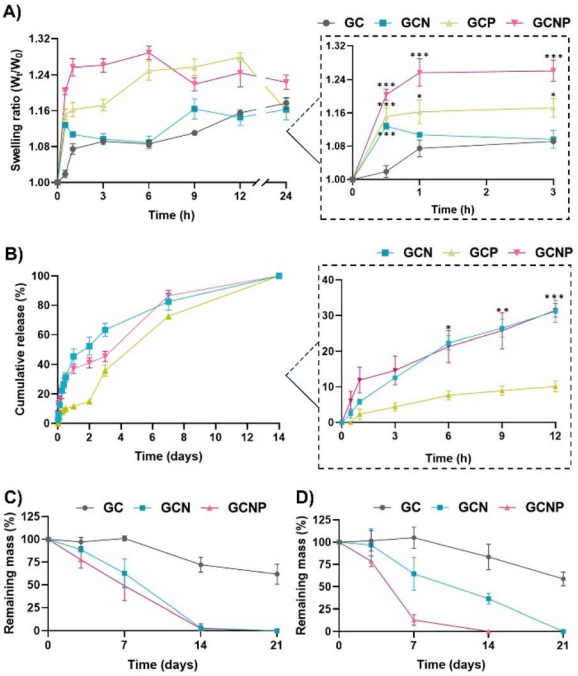

Fig. 4 Swelling behavior, release kinetics, and degradation profile of GC-based hydrogels. (A) Swelling ratio (W_t/W_0) over 24 hours, with a zoomed-in view of early time points (0–3 h) highlighting significant differences. (B) Cumulative release (%) of incorporated compounds over 14 days, with details of the first 12 hours. (C) Enzymatic degradation and (D) degradation mediated by RAW 264.7 cells over 21 days. Data are presented as mean ± standard error of the mean ($n = 3$). Asterisks indicate significant differences as follows: $p < 0.05$ (*), $p < 0.01$ (**), and $p < 0.001$ (***). Differences not marked with asterisks are not statistically significant.

stiffness of GCNP and the robust compressive strength and toughness of GCN suggest that these formulations provide mechanical resilience sufficient to support early bone healing in non-load-bearing defects.

2.4 Swelling behavior

The swelling ratio of hydrogels is essential for tissue engineering applications since it directly influences their ability to support cell infiltration and nutrient transport.[42] The swelling characteristics, critical for nutrient transport and drug release, were evaluated over 24 hours (Fig. 4A). GC hydrogels exhibited minimal swelling, indicative of a compact network. NAC and PAMP significantly increased the swelling capacity in GCN and GCNP hydrogels, with GCNP achieving the highest swelling ratio. This suggests synergistic interactions between NAC and PAMP, which promotes a more hydrated and porous polymer matrix, ideal for drug delivery and tissue integration.

2.5 Cumulative release and degradation profiles

Cumulative release studies demonstrated distinct profiles across formulations. GCP hydrogels exhibited the slowest release, favoring prolonged drug retention. GCN hydrogels showed a pronounced initial burst release within the first 48 hours, followed by sustained diffusion. GCNP hydrogels achieved a balance between an initial burst and a steady release phase, demonstrating the synergistic modulation of drug release kinetics by NAC and PAMP. These results highlight the impact of hydrogel composition on drug release kinetics, with GCN showing the most robust release, GCNP providing balanced kinetics, and GCP delivering a slower, more controlled release.

Hydrogel degradation was analyzed in the presence of RAW264.7 macrophages and lysozyme (Fig. 4C and D). GC hydrogels degraded the slowest, retaining over 75% of their mass by day 21. The incorporation of NAC and PAMP accelerated degradation, with GCNP hydrogels showing the fastest breakdown.

2.6 *In vitro* cell viability

The biocompatibility and effect of the hydrogels on cell proliferation were evaluated using an MTT assay with MC3T3-E1 preosteoblastic cells over 1, 3, and 5 days (Fig. 4A). GCN and GCP hydrogels exhibited an initial decrease in metabolic activity during the first 24 hours, which may be attributed to a transient cellular stress response caused by the interaction with hydrogel components. However, GCNP hydrogels showed a significant and sustained increase in metabolic activity over time, suggesting that the combination of NAC and PAMP has a synergistic effect that enhances cell proliferation and metabolic function. These results indicate that the incorporation of bioactive molecules into GCNP hydrogels not only mitigates the initial stress response but also promotes long-term cell viability, emphasizing their suitability as scaffolds for BTE.

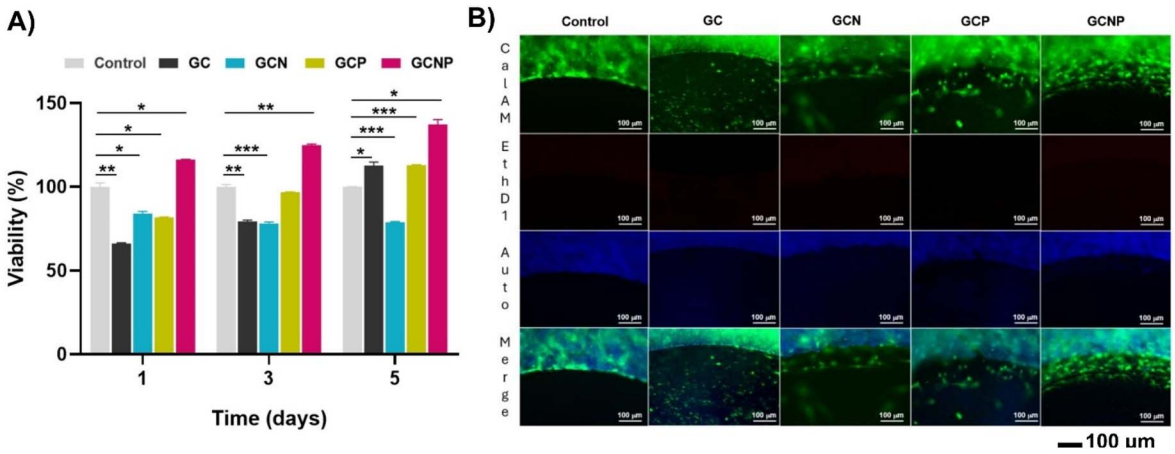

Fig. 5 *In vitro* and *ex vivo* viability of GC-based hydrogels. (A) Metabolic activity of MC3T3-E1 cells cultured with GC, GCN, GCP, and GCNP hydrogels, evaluated by MTT assay at days 1, 3, and 5. Results are expressed as percentages relative to monolayer control ($n = 3$). (B) Representative fluorescence images of calvarial bone explants cultured *ex vivo* in contact with the hydrogels, stained with a Live/Dead viability kit. Live cells appear green (Calcein-AM), dead cells red (EthD-1), and blue corresponds to tissue autofluorescence. Data are presented as mean ± standard error of the mean. Asterisks indicate statistically significant differences: $p < 0.05$ (*), $p < 0.01$ (**), and $p < 0.001$ (***). Differences not marked with asterisks are not statistically significant. Scale bars: 100 µm.

2.7 *Ex vivo* viability in critical size calvaria defects

To assess biocompatibility and tissue integration, *ex vivo* cell viability was analysed in critical size calvaria defects using a LIVE/DEAD assay (Fig. 5B). Green fluorescence from intracellular esterase activity (calcein AM) indicated live cells, while red fluorescence from ethidium homodimer-1 marked dead cells. No red fluorescence was detected in any hydrogel formulation, confirming their high biocompatibility. Additionally, blue autofluorescence highlighted the surrounding bone tissue, while overlapping green fluorescence demonstrated cell growth and tissue viability within the defect.

Among all hydrogel formulations, GCNP hydrogels showed the most pronounced cellular infiltration and viability, evidenced by the dense green fluorescence surrounding the defect site. This enhanced tissue response underscores the potential of GCNP hydrogels to support cell survival and promote integration within the bone environment. These findings further validate their application in bone tissue regeneration.

2.8 *In vitro* and *ex vivo* mineralization

The osteogenic capacity of the hydrogels was assessed *in vitro* and *ex vivo* using Alizarin Red S (ARS) and alkaline phosphatase (ALP) staining to determine calcium deposition and osteoblast differentiation, respectively (Fig. 6A). Among all formulations, GCNP hydrogels exhibited the highest intensity of ARS and ALP staining, indicating high mineralization and osteogenic activity. GCN and GCP hydrogels also enhanced mineralization compared to GC hydrogels, but to a lesser extent than GCNP. Quantitative analysis of ARS staining confirmed that GCNP hydrogels promoted the largest mineralized area among all groups, demonstrating superior capacity to support calcium deposition (Fig. 6B). Similarly, *ex vivo* mineralization was assessed through fluorescence imaging of ARS-stained calvarial sections (Fig. 6C). GCNP hydrogels induced the most pronounced mineral deposition at the defect site, as suggested by more extensive ARS staining.

GCN and GC hydrogels also supported mineralization, though to a lesser extent. Minimal mineralization was observed in the negative control, while the positive control displayed robust calcium deposition. Collectively, these findings suggest that GCNP hydrogels enhance osteoblast differentiation and mineral deposition, highlighting their potential as scaffolds for bone regeneration. The combination of NAC and PAMP within GCNP hydrogels appears to contribute to their bioactivity, making them promising candidates for further exploration in BTE applications.

3. Discussion

Bone tissue engineering aims to develop biomaterials that support bone regeneration by mimicking the extracellular matrix and promoting cellular activities crucial for tissue repair.[5,6,43–46] Traditional approaches often rely on ceramic- or metal-based scaffolds, but their limitations—such as brittleness, lack of bioactivity, and poor biodegradability—have driven interest in polymer-based hydrogels as alternative scaffolds[43,47]

Although the SEM images correspond to the lyophilized hydrogels, and thus the microstructure may not exactly reflect the hydrated state in contact with cells or tissues, they allowed us to observe the effect of NAC on porosity and to compare the hydrogel formulations under the same preparation conditions. The combined use of methacrylate gelatin and chitosan ensures the formation of a stable, covalently crosslinked 3D network, leveraging the biocompatibility of natural polymers while improving their mechanical and structural properties.[39,48] In contrast to other reported hydrogels synthesized using GelMA : ChMA ratios of 2 : 1 and 1 : 2, which resulted in smaller pore sizes (2–30 µm),[37] our synthesis conditions yielded significantly larger pores, reaching up to 212 µm. This enhancement highlights the critical role of NAC as a structural modulator, promoting a more open and porous network that is particularly

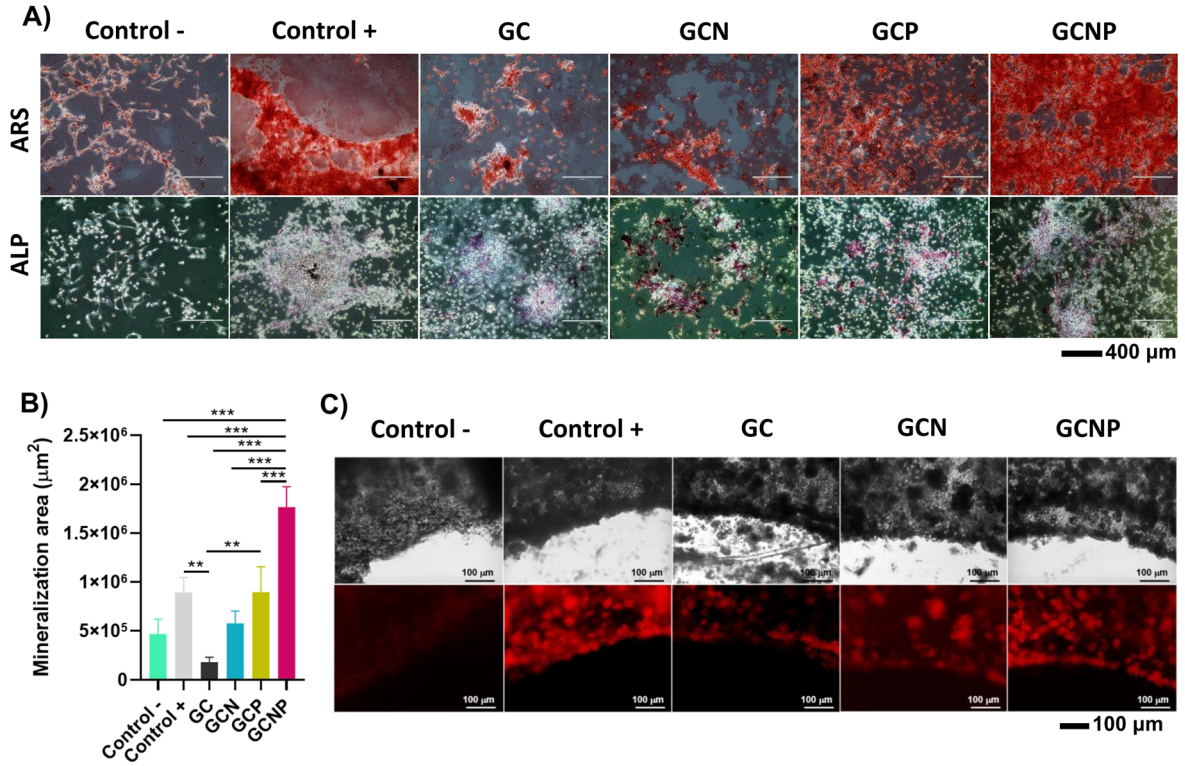

Fig. 6 *In vitro* and *ex vivo* evaluation of osteogenic activity induced by GC-based hydrogels. (A) Representative images of MC3T3-E1 cells after 14 days of osteogenic differentiation, stained for calcium deposition (ARS) and alkaline phosphatase activity (ALP). Control – corresponds to cells in growth medium, and control + to cells cultured with osteogenic medium with insulin. Scale bars: 400 μm. (B) Quantification of mineralized area from ARS staining ($n = 3$). (C) Fluorescence images of calvarial bone explants cultured *ex vivo* with hydrogels under osteogenic conditions. Data are presented as mean ± standard error of the mean. Asterisks indicate statistically significant differences: $p < 0.05$ (*), $p < 0.01$ (**), and $p < 0.001$ (***). Differences not marked with asterisks are not statistically significant. Scale bars: 100 μm.

advantageous for BTE.[40] Reactive thiol groups (-SH) of NAC interact with free radicals during photopolymerization, forming thiol-methacrylate bonds that introduce additional crosslinking points. This process creates more flexible segments, reduces network compaction, and results in a more porous structure. Additionally, carboxyl and amine groups of NAC influence polymer organization during polymerization, further contributing to the formation of an open, interconnected network.[28] Larger pores, as achieved in our hydrogels, facilitate nutrient diffusion, angiogenesis, and cellular infiltration—critical factors for effective extracellular matrix deposition and tissue regeneration.

The mechanical properties of GCNP hydrogels, while lower than those of native bone tissue (trabecular bone: 10–3000 MPa Young's modulus, 0.1–30 MPa compressive strength; cortical bone: 17–20 GPa Young's modulus, 115–205 MPa compressive strength),[49] GCNP hydrogels exhibited a Young's modulus of 55.26 ± 5.79 kPa and a compressive strength of 44.31 kPa, values consistent with hydrogel scaffolds designed for non-load-bearing bone defects. In such applications, compressive strengths in the range of 10–1000 kPa are generally sufficient to maintain scaffold integrity and support tissue infiltration and regeneration.[21,50] Therefore, the moderate stiffness of our hydrogels—coupled with high porosity and sustained bioactive release—could promote a dynamic biomechanical environment for stem cell adhesion, osteogenic commitment, and effective bone mineralization in non-load-bearing defects. In comparison to alternative formulations, the superior mechanical resilience of GCNP hydrogels indicates that the synergistic effects of NAC and PAMP not only enhance bioactivity but also optimize structural properties.

Swelling behavior is a critical parameter for hydrogels used in tissue engineering and drug delivery systems, as it influences both nutrient transport and drug release kinetics.[51] The incorporation of NAC and PAMP significantly enhanced the swelling capacity of GCNP hydrogels, supporting a more hydrated and porous polymer matrix. This increased swelling expands the pores of hydrogels, facilitating cellular infiltration and controlled drug diffusion.[52] Furthermore, water uptake relaxes polymer chains, allowing gradual hydrogel volume expansion, which plays a pivotal role in regulating the release kinetics of encapsulated bioactive molecules.[53] The cumulative drug release profile of GCNP hydrogels demonstrated a controlled balance between an initial burst release and sustained diffusion. The initial burst, facilitated by interactions between NAC and the polymer matrix, provides a rapid therapeutic concentration during early tissue healing phases.[54] The subsequent sustained release phase ensures prolonged bioactivity, aligning with the dynamic requirements of bone tissue regeneration.[46] This intermediate release profile, balancing rapid diffusion with long-term delivery, outperformed GCN and GCP hydrogels,

highlighting the synergistic effect of NAC and PAMP in achieving effective drug release kinetics.[55]

The complete degradation of the GCNP hydrogels occurred within approximately two weeks, which is faster than the full-time frame required for complete bone regeneration, generally spanning several weeks to months depending on the defect and anatomical site.[56] However, this degradation profile was designed to provide a burst release of bioactive compounds (NAC and PAMP) during the critical early phases of bone healing, including the inflammatory, cell recruitment, and early matrix deposition stages, which typically occur within the first 2–3 weeks.[57] While slower degradation might be advantageous for providing prolonged mechanical support in load-bearing defects, the non-load bearing calvaria defect model used in this study does not require long-term structural reinforcement. Therefore, the fast-degrading GCNP hydrogels serve as a temporary matrix to modulate the local biological environment during the initial healing phase, after which the native bone remodeling processes continue.

The *in vitro* and *ex vivo* assays demonstrated excellent biocompatibility and improved cell viability, proliferation, and tissue integration. GCN and GCP hydrogels slightly reduced cell viability at 24 hours, however, over time, cell proliferation increased, showing the influence of the active molecules within the hydrogel. The combination of NAC and PAMP in the GCNP formulation enhanced the capacity of the molecules to promote cell survival and cell proliferation, consistent with the reported roles of NAC and PAMP in tissue repair.[25,27]

GCNP hydrogels exhibited the highest osteogenic potential across all formulations, as evidenced by the increased mineralization and osteoblast differentiation *in vitro* and *ex vivo*. The strong ARS and ALP staining in GCNP hydrogels highlights their capacity to promote calcium deposition and osteoblast activity, beyond the previously reported hydrogels.[29,30,32,33] The synergistic effects of NAC, which has been reported to support osteogenic differentiation, and PAMP, which may contribute to vascularization and tissue healing, likely play a role in this enhanced performance.[31,58] These results position GCNP hydrogels as promising candidates for BTE, as they support mineral deposition and osteoblast activity, suggesting potential osteogenic properties that warrant further investigation.

4. Experimental

4.1 Synthesis of hydrogels

To synthesize chitosan methacrylate (ChMA), 1.5% chitosan (BioBasic, CB0660) was solubilized in 2% acetic acid (J.T. Baker, 9508-02) and stirred for 18 h. Then, an excess molar 1 : 6 of methacrylic anhydride (Sigma-Aldrich, 276685) was added, and the reaction continued for 24 hours at 40 °C, accordingly.[59] For gelatin methacrylation a 10% gelatin (Sigma-Aldrich, G1890) solution in PBS 1X was adjusted to pH 9 using 5 M NaOH. Methacrylate was added using the sequential method reported by Shirahama *et al.*, at 0.1 mL g^{-1}, stirring at 500 rpm for 3 hours at 40 °C, protected from light.[22] Afterward, the reaction mixture was diluted with a 1 : 5 ratio of phosphate buffer solution to stop the reaction homogenized for 5 minutes while stirring. The unreacted methacrylic anhydride was removed by dialysis (12–14 kDa) over four days with regular water exchanges. Each final product was frozen and freeze-dried.[48,60]

Hydrogels were prepared from 4% GelMA and 3% ChMA in a 3 : 1 ratio (GC), selected following a series of preliminary tests aimed at ensuring room-temperature injectability (Fig. S1†). The ratio was optimized by evaluating gelation at 1 : 1, 2 : 1, and 3 : 1 GelMA : ChMA.[37,39] All three ratios formed gels upon UV irradiation, with the 3 : 1 ratio providing superior consistency (results not shown). To crosslink the polymers, 0.2% (w/v) lithium phenyl-2,4,6-trimethylbenzoylphosphinate (LAP) (Sigma-Aldrich, 900889) was added, followed by exposure to UV light for 60 seconds. The GCN hydrogels were loaded with *N*-acetylcysteine (NAC) (Sigma-Aldrich, A7250) at 20 mM, after evaluating its DPPH radical scavenging capacity (Fig. S2†), which is consistent with concentrations used in hydrogels for wound healing.[28] The concentration of pro-adrenomedullin peptide (PAMP) (TOCRIS, 6552) used in the GCP hydrogels (50 μg mL^{-1}) was selected considering the high biological potency of PAMP compared to AM and prior studies on AM delivery. In a bone regeneration model, systemic administration of over 160 μg of AM(27–52) over four weeks produced significant anabolic effects in bone.[61] As PAMP exerts biological activity at significantly lower concentrations,[34] a lower PAMP dose 50 μg mL^{-1} was selected. GCNP hydrogels were prepared using a combination of NAC and PAMP.

4.2 SEM and FTIR

To investigate the formation of functional groups within the polymer structure, the hydrogels were frozen and lyophilized for further processing. The surface structure and cross-sections of the scaffolds were examined using scanning electron microscopy (SEM) with an JSM-7800F (JEOL) at 1 kV, under variable pressure conditions. The chemical composition of the scaffolds was analyzed using an FT-IR spectrophotometer (Agilent Cary 630, ATR cell) over a range of 600 to 4000 cm^{-1}.

4.3 Mechanical testing

The mechanical properties of hydrogels were characterized by Young's modulus (ε), compression strength (σF), and toughness. Compression tests were performed using a texture analyzer (Brookfield CT3-10kg, AMETEK Brookfield, Middleboro, MA, USA) equipped with a cylindrical probe (TA11/1000, 25.4 mm D, 35 mm H). The hydrogels with 6 mm in diameter were pre-hydrated. They were placed on a flat plate at room temperature and compressed at a constant descent speed of 0.5 mm s^{-1}.[62] From the stress–strain curves, ε was calculated as the slope of the linear region, σF as the maximum stress value a material can withstand before the first failure. Furthermore, toughness was calculated as the area under the curve to obtain the energy absorbed up to the point of failure.

4.4 Swelling ratio and drug release profiles

The hydrogels were weighed before incubation with 1× PBS at 37 °C for varying durations and 100 rotation per min (rpm) in an incubating shaker. At each time point, the PBS was removed

and collected, then hydrogels were weighed. The swelling ratio was calculated using the following formula:[24]

$$\text{Swelling ratio} = \frac{W_t}{W_0} \quad (1)$$

where W_t was the weight of the swelling hydrogels, and W_0 was the weight of the original hydrogel.

As the hydrogels swelled, the encapsulated drugs were gradually released. To determine the release profile, samples were extracted from the collected PBS containing NAC, PAMP, or both, at scheduled intervals for 14 days. The ninhydrin (Sigma-Aldrich, N4876) reaction, commonly used to characterize amino acids and peptides, was employed to quantify the free amino groups (NH_2) released from the hydrogels.[63] The concentrations of NAC and PAMP were measured using the ninhydrin assay at a wavelength of 570 nm and interpolated in a glycine standard curve to obtain the cumulative release (%) plotted against time using the next formula:

$$\text{Cumulative release}(\%) = \frac{M_t}{M_\infty} \times 100 \quad (2)$$

where M_t was the amount released from a sample at time t.

4.5 Degradation profile

The initial weights of the hydrogels were recorded after reaching equilibrium (W_o) and then incubated in 1× PBS with lysozyme (10 000 U L^{-1}) (Sigma-Aldrich, 62970) similar to circulating blood, at 37 °C for 1, 3, 7, 14, and 21 days.[64] The degradation solution was replaced every two days. At the end of the incubation periods, the scaffolds were freeze-dried, and their weights were recorded (W_t). The percentage of degradation was calculated using the following formula:

$$\text{Degradation}(\%) = \frac{W_0 - W_t}{W_0} \times 100 \quad (3)$$

where W_t was the weight of the hydrogels at time t, and W_0 was the weight of the initial hydrogel.

4.6 Cell culture

Pre-osteoblastic MC3T3-E1 cells were seeded in 24-well plates at a density of approximately 7500 cells per well. After 24 hours, hydrogels were prepared in transwells with a pore size of 0.4 μm and maintained in culture with cells for 24 and 48 hours. To assess cell viability, MTT (0.5 mg mL^{-1}) was added to each well and incubated at 37 °C for 4 hours. The resulting purple formazan was dissolved using a 0.1 M HCl/10% SDS solution. The optical density (OD) of each well was measured using a microplate reader at a wavelength of 570 nm (EPOCH, BioTek). Cell viability was obtained from the next formula:

$$\text{Cell viability}(\%) = \frac{\text{Abs}_{\text{sample}} - \text{Abs}_{\text{blanc}}}{\text{Abs}_{\text{control}} - \text{Abs}_{\text{blanc}}} \times 100 \quad (4)$$

Bone marrow from an 8 weeks-old mouse was collected from the femur and tibia by flushing with 1× PBS according to Amend *et al.* 2016.[65] All animal procedures were performed in accordance with the Guidelines for Care and Use of Laboratory Animals of the Centre for Scientific Research and Higher Education of Ensenada, Baja California (CICESE) and approved by the Bioethics Committee with the number: 8C.17DBEA/DIR-O/091. The cells were incubated with α-MEM medium containing 10% FBS and 1% antibiotic-antimycotic for 48 hours under standard culture conditions. Adherent cells were then collected and seeded at a density of 45 000 cells per well in a 24-well plate. After 24 hours of incubation, a differentiation medium containing 25 μg mL^{-1} L-ascorbate and 5 mM β-glycerophosphate was added, along with hydrogels in transwells. The medium was changed every three days for 21 days, after which staining with Alizarin Red S (ARS, WAKO, 015-01151) and alkaline phosphatase (ALP, Sigma-Aldrich, 86R-1KT).

4.7 Calvaria culture

Four-day-old mice were euthanized following the guidelines of the critical size defect (CSD) model for mouse calvaria bone with some modifications.[66] The calvariae were aseptically dissected and sectioned along the sagittal and coronal sutures. Each quarter of the calvaria was placed in a 48-well tissue culture plate containing Dulbecco's Modified Eagle's Medium (DMEM, Corning) supplemented with 0.1% bovine serum albumin (BSA) (Biotech, AO0023), 1% penicillin/streptomycin (Sigma-Aldrich), and insulin (Sigma-Aldrich, 16634) as a positive control for mineralization. Calvariae were cultured for one day before creating full-thickness circular defects, 2 mm in diameter, following previous reports with some modifications.[67,68] Hydrogels were placed in the CSD area. The calvariae, with hydrogels in place, were cultured concave side down on the plate for two weeks, with media changes every two days. After 14 days, calvariae were stained using a Live/Dead Kit (Sigma-Aldrich, 04511), Alizarin Red (ARS), and Alkaline Phosphatase (ALP).

4.8 Mineralization assays

Cells and tissue were fixed with 4% paraformaldehyde (PFA) for 20 minutes. After rinsing the wells with distilled water, 2% ARS pH 4.2 solution was added and incubated at room temperature for 3 minutes – protected from light. Following the staining, the wells were rinsed with distilled water until no excess dye was visible. ALP staining was performed according to the manufacturer's protocols.

4.9 Statistical analysis

All experimental results are presented as mean ± standard deviation (SD) or standard error of the mean (SEM), as specified in each figure legend. Statistical analysis was performed using GraphPad Prism version 8.0.2 (GraphPad Software, San Diego, CA, USA). Comparative analyses for porosity and mechanical properties were conducted using one-way ANOVA. Viability and mineralization assays were also analyzed using one-way ANOVA, while swelling ratio, cumulative release, and degradation data were evaluated using two-way ANOVA. Tukey's post-hoc test was applied to determine statistically significant differences, with $p < 0.05$ considered significant. In all figures, asterisks denote significance levels as follows: * for $p < 0.05$, ** for $p < 0.01$, and

*** for $p < 0.001$. Non-significant differences between groups are not shown.

5. Conclusions

We developed and characterized gelatin methacrylate–chitosan methacrylate (GC) hydrogels with NAC and PAMP using UV-induced polymerization. NAC played a dual role by modifying the porous structure during crosslinking and later becoming bioactive as the hydrogel degraded. Its radical-scavenging activity promoted additional crosslinking points, increasing hydration and forming a more interconnected network. The incorporation of NAC enhanced not only pore size and swelling but also mechanical strength, improving compressive resistance without compromising stability—key for applications in bone tissue engineering. GCNP hydrogels showed excellent biocompatibility and promoted osteoblast viability and mineralization both *in vitro* and *ex vivo*, likely due to the combined action of NAC and PAMP. Their release profile offers both initial and sustained delivery, supporting dynamic bone healing processes. These results suggest that GCNP hydrogels are promising candidates for bone regeneration, combining mechanical robustness with biological functionality. However, further *in vivo* studies are needed to confirm their osteogenic and angiogenic potential.

Data availability

The data supporting this article have been included as part of the ESI.†

Author contributions

Tonatzin Zertuche-Arias: writing – review & editing, writing – original draft, methodology, formal analysis, data curation, conceptualization, investigation, visualization. Manuel Alatorre-Meda: resources, formal analysis, data curation, writing – review & editing. Ignacio A. Rivero: resources. Patricia Juárez: writing – review & editing, resources, conceptualization, formal analysis, project administration, supervision, visualization, funding Sources. Ana B. Castro-Ceseña: writing – review & editing, resources, conceptualization, formal analysis, project administration, supervision, visualization, funding Sources.

Conflicts of interest

The authors declare that they have no known financial or personal conflicts of interest that could have influenced the work reported in this paper.

Acknowledgements

This work was supported by CICESE (Grant No. 685105) to Patricia Juárez and CICESE (Grant no. 685112) to Ana B. Castro-Ceseña. SECIHTI also supported the work by providing a scholarship to Tonatzin Zertuche-Arias (grant no. 746304). We thank Lucía Michelle Chávez-López, Daniel Reyes-López, and Vanessa Rodríguez-Magaña, from Universidad Xochicalco for their valuable assistance in the experimental procedures. We also thank Marco A. Uriosegui for his support in fine-tuning the images required for publication.

References

1 S. H. Ralston, *Medicine*, 2017, **45**, 560–564.
2 A.-M. Wu, *Lancet Healthy Longev.*, 2021, **2**, 580–592.
3 R. Dimitriou, E. Jones, D. McGonagle and P. V. Giannoudis, *BMC Med.*, 2011, **9**, 66.
4 M. P. Nikolova and M. S. Chavali, *Bioact. Mater.*, 2019, **4**, 271–292.
5 M. M. Stevens, *Mater. Today*, 2008, **11**, 18–25.
6 P. Dec, A. Modrzejewski and A. Pawlik, *Int. J. Mol. Sci.*, 2023, **24**, 529.
7 Y. Tu, N. Chen, C. Li, H. Liu, R. Zhu, S. Chen, Q. Xiao, J. Liu, S. Ramakrishna and L. He, *Acta Biomater.*, 2019, **90**, 1–20.
8 A. Mandal, J. R. Clegg, A. C. Anselmo and S. Mitragotri, *Bioeng. Transl. Med.*, 2020, **5**, 1–12.
9 L. Zhao, Y. Zhou, J. Zhang, H. Liang, X. Chen and H. Tan, *Pharmaceutics*, 2023, **15**, 2514.
10 B. Kaczmarek, K. Nadolna and A. Owczarek, *The Physical and Chemical Properties of Hydrogels Based on Natural Polymers*, Elsevier Inc., 2019.
11 M. P. Das, P. R. Suguna, P. Karpunam, J. V. Vijaylakshmi and M. Renuka, *Int. J. Pharm. Pharm. Sci.*, 2017, **9**(9), 239–242.
12 D. Liu, M. Nikoo, G. Boran, P. Zhou and J. M. Regenstein, *Annu. Rev. Food Sci. Technol.*, 2015, **6**, 527–557.
13 B. J. Klotz, D. Gawlitta, A. J. W. P. Rosenberg, J. Malda and P. W. Melchels, *Trends Biotechnol.*, 2018, **34**, 394–407.
14 L. Michelini, L. Probo, S. Farè and N. Contessi Negrini, *Mater. Lett.*, 2020, **272**, 127865.
15 R. A. Batista, C. G. Otoni and P. J. P. Espitia, *Fundamentals of Chitosan-Based Hydrogels: Elaboration and Characterization Techniques*, Elsevier Inc., 2019, vol. 1.
16 A. Irastorza, I. Zarandona, M. Andonegi, P. Guerrero and K. de la Caba, *Food Hydrocolloids*, 2021, **116**, 106633.
17 S. M. Bashir, G. Ahmed Rather, A. Patrício, Z. Haq, A. A. Sheikh, M. Z. ul, H. Shah, H. Singh, A. A. Khan, S. Imtiyaz, S. B. Ahmad, S. Nabi, R. Rakhshan, S. Hassan and P. Fonte, *Materials*, 2022, **15**, 6251.
18 E. Jabbari, *Gels*, 2019, **5**, 30.
19 X. Zhao, X. Chen, H. Yuk, S. Lin, X. Liu and G. Parada, *Chem. Rev.*, 2021, **121**, 4309–4372.
20 V. S. Ghorpade, *Preparation of Hydrogels Based on Natural Polymers via Chemical Reaction and Cross-Linking*, Elsevier Inc., 2019.
21 K. Yue, G. T. Santiago, A. Tamayol, N. Annabi, A. Khademhosseini, W. Hospital, S. Arabia, G. Trujillo-de Santiago, M. M. Alvarez, A. Tamayol, N. Annabi and A. Khademhosseini, *Biomaterials*, 2016, **73**, 254–271.
22 H. Shirahama, B. H. Lee, L. P. Tan and N. J. Cho, *Sci. Rep.*, 2016, **6**, 31036.
23 P. Joshi, M. S. U. Ahmed, K. Vig, I. B. Vega Erramuspe and M. L. Auad, *Polym. Adv. Technol.*, 2021, **32**, 2229–2239.

24 H. Kim, K. Kim, B. Kim, K. Lee and S. Lee, *Korean J. Intern. Med.*, 2019, **34**, 210–219.
25 Z. Meng, J. Liu, Z. Feng, S. Guo, M. Wang, Z. Wang, Z. Li, H. Li and L. Sui, *Stem Cell Res. Ther.*, 2022, **13**, 466.
26 X. Liu, Y. Hou, M. Yang, X. Xin, Y. Deng, R. Fu, X. Xiang, N. Cao, X. Liu, W. Yu, B. Yang and Y. Zhou, *Adv. Healthcare Mater.*, 2023, **12**, 2300890.
27 C. H. Lin, K. F. Lin, K. Mar, S. Y. Lee and Y. M. Lin, *Tissue Eng., Part C*, 2016, **22**, 792–800.
28 L. S. Gomez-Aparicio, J. Bernáldez-Sarabia, T. A. Camacho-Villegas, P. H. Lugo-Fabres, N. E. Díaz-Martínez, E. Padilla-Camberos, A. Licea-Navarro and A. B. Castro-Ceseña, *Biomater. Sci.*, 2020, **9**, 726–744.
29 D. Naot, K. E. Callon, A. Grey, G. J. S. Cooper, I. R. Reid and J. Cornish, *Endocrinology*, 2001, **142**, 1849–1857.
30 S. Martínez-Herrero, I. M. Larrayoz, L. Ochoa-Callejero, L. J. Fernández, A. Allueva, I. Ochoa and A. Martínez, *Front. Physiol.*, 2016, **7**, 280.
31 T. Kukita, H. Hiura, J. Y. Gu, J. Q. Zhang, Y. Kyumoto-Nakamura, N. Uehara, S. Murata, S. Sonoda, T. Yamaza, I. Takahashi and A. Kukita, *Lab. Invest.*, 2021, **101**, 1449–1457.
32 D. S. Musson, J. L. McLachlan, A. J. Sloan, A. J. Smith and P. R. Cooper, *Biol. Cell.*, 2010, **102**, 145–157.
33 F. Wang, W. Wang, L. Kong, L. Shi, M. Wang, Y. Chai, J. Xu and Q. Kang, *Front. Cell Dev. Biol.*, 2021, **9**, 649277.
34 A. Martínez, E. Zudaire, S. Portal-Núñez, L. Guédez, S. K. Libutti, W. G. Stetler-Stevenson and F. Cuttitta, *Cancer Res.*, 2004, **64**, 6489–6494.
35 V. Roldós, R. J. Carbajo, A. K. Schott, A. Pineda-Lucena, L. Ochoa-Callejero, A. Martínez, A. Ramos and B. De Pascual-Teresa, *Eur. J. Med. Chem.*, 2012, **55**, 262–272.
36 D. F. S. Fonseca, P. C. Costa, I. F. Almeida, P. Dias-Pereira, I. Correia-Sá, V. Bastos, H. Oliveira, C. Vilela, A. J. D. Silvestre and C. S. R. Freire, *Macromol. Biosci.*, 2020, **20**, 2000195.
37 S. M. Saraiva, S. P. Miguel, M. P. Ribeiro, P. Coutinho and I. J. Correia, *RSC Adv.*, 2015, **5**, 63478–63488.
38 W. Kwon and E. Jeong, *Polymers*, 2020, **12**, 1461.
39 A. R. Osi, H. Zhang, J. Chen, Y. Zhou, R. Wang, J. Fu, P. Müller-Buschbaum and Q. Zhong, *ACS Appl. Mater. Interfaces*, 2021, **13**, 22902–22913.
40 F. Mukasheva, L. Adilova, A. Dyussenbinov, B. Yernaimanova, M. Abilev and D. Akilbekova, *Front. Bioeng. Biotechnol.*, 2024, **12**, 1444986.
41 B. Thavornyutikarn, N. Chantarapanich, K. Sitthiseripratip, G. A. Thouas and Q. Chen, *Prog. Biomater.*, 2014, **3**, 61–102.
42 K. Xu, H. Yao, D. Fan, L. Zhou and S. Wei, *Carbohydr. Polym.*, 2021, **254**, 117286.
43 S. Yue, H. He, B. Li and T. Hou, *Nanomaterials*, 2020, **10**, 1511.
44 H. Shi, K. Zhou, M. Wang, N. Wang, Y. Song, W. Xiong, S. Guo, Z. Yi, Q. Wang and S. Yang, *Theranostics*, 2023, **13**, 3245–3275.
45 F. M. Chen and X. Liu, *Prog. Polym. Sci.*, 2016, **53**, 86–168.
46 A. D. Anupama, S. Ray, U. Arora, S. Mitra, A. Sionkowska and A. K. Jaiswal, *Front. Bioeng. Biotechnol.*, 2022, **10**, 969843.
47 S. Hou, X. Wang, S. Park, X. Jin and P. X. Ma, *Adv. Healthcare Mater.*, 2015, **4**, 1491–1495.
48 X. Luo, Y. Liu, J. Pang, S. Bi, Z. Zhou, Z. Lu, C. Feng, X. Chen and M. Kong, *Carbohydr. Polym.*, 2020, **236**, 116067.
49 E. F. Morgan, G. U. Unnikrisnan and A. I. Hussein, *Annu. Rev. Biomed. Eng.*, 2018, **20**, 119–143.
50 S. Chai, J. Huang, A. Mahmut, B. Wang and Y. Yao, *Front. Bioeng. Biotechnol.*, 2022, **10**, 875363.
51 L. Wang, K. Chen, H. Wen, D. Ouyang, X. Li, Y. Gao, W. Pan and X. Yang, *AAPS PharmSciTech*, 2017, **18**, 82–92.
52 E. M. Ahmed, *J. Adv. Res.*, 2015, **6**, 105–121.
53 A. Bertz, S. Wöhl-Bruhn, S. Miethe, B. Tiersch, J. Koetz, M. Hust, H. Bunjes and H. Menzel, *J. Biotechnol.*, 2013, **163**, 243–249.
54 G. N. Duda, S. Geissler, S. Checa, S. Tsitsilonis, A. Petersen and K. Schmidt-Bleek, *Nat. Rev. Rheumatol.*, 2023, **19**, 78–95.
55 A. W. Martinez, J. M. Caves, S. Ravi, W. Li and E. L. Chaikof, *Acta Biomater.*, 2014, **10**, 26–33.
56 T. A. Einhorn and L. C. Gerstenfeld, *Nat. Rev. Rheumatol.*, 2015, **11**, 45–54.
57 A. G. Robling, A. B. Castillo and C. H. Turner, *Annu. Rev. Biomed. Eng.*, 2006, **8**, 455–498.
58 M. Kaymakoglu, E. Ciftci, P. Korkusuz, E. Ozdemir, M. E. Erden and E. Turhan, *Acta Orthop. Traumatol. Turc.*, 2023, **57**, 221–228.
59 M. Zanon, A. Chiappone, N. Garino, M. Canta, F. Frascella, M. Hakkarainen, C. F. Pirri and M. Sangermano, *Mater. Adv.*, 2022, **3**, 514–525.
60 Y. Li, C. Liu, W. Liu, X. Cheng, A. Zhang, S. Zhang, C. Liu, N. Li and X. Jian, *Macromol. Biosci.*, 2021, **21**, 2100262.
61 J. Cornish, K. E. Callon, U. Bava, D. H. Coy, T. B. Mulvey, M. A. F. Murray, G. J. S. Cooper and I. R. Reid, *J. Endocrinol.*, 2001, **170**, 251–257.
62 F. Araiza-Verduzco, E. Rodríguez-Velázquez, H. Cruz, I. A. Rivero, D. R. Acosta-Martínez, G. Pina-Luis and M. Alatorre-Meda, *Materials*, 2020, **13**, 534.
63 M. Friedman, *J. Agric. Food Chem.*, 2004, **52**, 385–406.
64 R. S. Leena, M. Vairamani and N. Selvamurugan, *Colloids Surf., B*, 2017, **158**, 308–318.
65 S. R. Amend, K. C. Valkenburg and K. J. Pienta, *J. Visualized Exp.*, 2016, **2016**, 53936.
66 D. A. Horn and I. R. Garrett, *Biotech. Histochem.*, 2004, **79**, 151–158.
67 Y. Ji, L. Wang, D. C. Watts, H. Qiu, T. You, F. Deng and X. Wu, *Dent. Mater.*, 2014, **30**, 1263–1273.
68 X. Wu, L. U. Wang, F. Deng and D. C. Watts, *Microsc. Res. Tech.*, 2014, **1043**, 1037–1043.